# Interaction Between Diffusion and Michaelis-Menten Uptake of Dopamine After Iontophoresis in Striatum

Charles Nicholson
Department of Physiology and Biophysics, New York University Medical Center, New York, New York 10016 USA

ABSTRACT A quantitative description of the behavior of a neurotransmitter in the brain extracellular microenvironment requires an understanding of the relative importance of diffusion versus uptake processes. This paper models the behavior of dopamine released from a small iontophoresis electrode and its voltammetric detection by a carbon fiber sensor 100 μm away as a basis for developing a new paradigm for measuring dopamine kinetics in intact rat neostriatum. The diffusion equation incorporating uptake, characterized by a maximum velocity $V_{max}$ and a Michaelis-Menten constant $K_m$, was transformed to an integral equation and solved numerically for the dopamine concentration, $C$. Analytical solutions were derived for limiting cases of a steady-state free-boundary problem when $C \gg K_m$ and the linear time-dependent problem when $C \ll K_m$. These solutions were compared with complete numerical solutions, both for normal uptake ($V_{max}$ = 0.2 or 0.8 μM $s^{-1}$; $K_m$ = 0.15 μM), and in the presence of the uptake blocker nomifensine ($K_m$ = 6 μM). The results suggest that an experimental strategy for the quantitative analysis of dopamine, and other compounds, in living tissue is to fit a family of concentration versus time curves generated with different iontophoretic current strengths and recorded with a microsensor, to the numerical solution of the diffusion-uptake equation.

## INTRODUCTION

The diffusion of substances in the brain extracellular microenvironment has importance both for the transport of metabolic substrates and the transmission of signals via nonsynaptic communication (Nicholson, 1979; Schmitt, 1984; Nicholson and Rice, 1991). This latter modality has also been termed "volume transmission" (Fuxe and Agnati, 1991) and "nonsynaptic diffusion neurotransmission" (Bach-y-Rita, 1993). The importance of such extracellular interactions for G protein-coupled mechanisms has been postulated by Hille (1992), whereas other recent papers have demonstrated that both GABA (Isaacson et al., 1993) and NO (Schuman and Madison, 1994) can function as extra-synaptic signals. But diffusion alone, as a mechanism of signal propagation, has limitations, because diffusing molecules eventually reach all sites unless physically impeded by barriers. To effectively use communication via the brain extracellular microenvironment, an uptake or inactivation process, which may itself be subject to physiological regulation, is desirable. One of the best known examples where both diffusion and uptake interact to control the spatial and temporal distribution of a neuroactive substance is the dopaminergic system of the neostriatum. This system gains especial interest because of its role in Parkinson's disease.

Parkinson's disease can be alleviated by strategies that provide a diffuse and tonic supply of dopamine (DA) to the striatum (Winn et al., 1989). This observation suggests that in the normal striatum DA released from a presynaptic site has actions beyond the immediate postsynaptic receptors. Yet it is also known that there is an avid uptake system located predominantly in the presynaptic terminals (Holz and Coyle, 1969; Justice et al., 1988; Horn, 1990; Hitri et al., 1994) that should function to restrict severely the spatial distribution of synaptically released DA.

To reconcile these and other facts about the neostriatum, it is necessary to characterize precisely the relative roles of diffusion and uptake in living striatal tissue. The technique of fast-scan cyclic voltammetry (FCV) provides that capability and has been used effectively in the striatum, particularly in the laboratory of Wightman and co-workers (e.g., Kelly and Wightman, 1987; Near et al., 1988; May et al., 1988; Wightman et al., 1988; Wightman and Zimmerman, 1990; Kennedy et al., 1992a, b; Kawagoe et al., 1992; Garris and Wightman, 1994a), where the uptake process has been studied using stimulation of the median forebrain bundle to activate a volume of synapses and so provide a source of DA. As valuable as this method is, it has the shortcoming that the source is incompletely defined in space and time. Another approach uses pressure ejection of DA from a micropipette combined with chronoamperometric detection (Van Horne et al., 1992; Luthman et al., 1993; Cass et al., 1993). This provides a better-defined source, however precise control is difficult and the theory has yet to be described, so the data must presently be treated in a qualitative manner. The recent ad hoc model proposed by Cass et al. (1993) to compare regional variations in sensitivity to uptake inhibitors does not address adequately the complexities of the problem (see Rice and Nicholson (1995) for further discussion).

An approach that has the potential to remove the limitations of the previous methods is to use a micro-iontophoretic source to precisely release DA and then measure the arrival of this substance at a separate carbon fiber microelectrode using FCV, which provides sufficient time resolution and confirms the identity of the DA. The method requires a complete mathematical solution of the three-dimensional

*Received for publication 25 July 1994 and in final form 20 December 1994.*
Address reprint requests to Dr. C. Nicholson, Department of Physiology and Biophysics, New York University Medical Center, 550 First Ave., New York, NY 10016. E-mail: nicholsn@is.nyu.edu.

0006-3495/95/05/1699/17 $2.00

diffusion problem with nonlinear uptake. This paper provides this solution and demonstrates its characteristics based on available diffusion and kinetic parameters. This theory can be applied (M. E. Rice and C. Nicholson, unpublished observation) to interpret experimental data obtained using DA iontophoresis in the normal striatal brain slice and in the 6-OHDA-lesioned rat striatum, which is an animal model of Parkinson's disease (Zigmond et al., 1992).

The present mathematical model is derived from previous work on diffusion from an iontophoretic point source (Nicholson and Phillips, 1981; Nicholson, 1992), but here the linear uptake term of the former work is replaced with a nonlinear expression describing Michaelis-Menten kinetics characterized by a rate constant $V_{max}$ ($\mu$M s$^{-1}$) and Michaelis-Menten constant $K_m$ ($\mu$M). Such kinetics, representing a high affinity uptake system in the presynaptic terminals, are now well accepted (Horn, 1979, 1990; Wightman and Zimmerman, 1990; Hitri et al., 1994). An interpretation of the kinetic constants has been provided by Horn: "The term $K_m$ ... is generally assumed to be a measure of the dissociation constant for the binding of substrate (DA) to the membrane uptake sites. Thus, the $K_m$ value may be taken as a reciprocal measure of the affinity of the substrate for the uptake sites. The $V_{max}$ is a measure of the number of amine uptake sites present, and it is dependent on the type and amount of tissue present. The $K_m$, however, is independent of the total number of uptake sites present" (Horn, 1979).

Some earlier studies (Shaskan and Snyder, 1970; Stamford et al., 1984, 1986; Mireylees et al., 1986) postulated an additional low affinity uptake system ($K_m$ = 8 $\mu$M; Stamford et al., 1984), but subsequently Wightman and co-workers dismissed this as an experimental artifact (Near et al., 1988; Wightman and Zimmerman, 1990).

The nonlinear partial-differential equation with Michaelis-Menten uptake describing the migration of DA has no analytical solution except in certain limiting cases, but it is analogous with the problem of oxygen consumption by a spherical cell, and literature on this topic provides a starting point for deriving the numerical solution to the present problem. Specifically, the integral equation approach of Tosaka and Miyake (1982) is used in this study.

This paper will: 1) provide a basis for the use of the diffusion equation together with Michaelis-Menten kinetics; 2) derive a numerical algorithm for the solution of this equation for the specific problem of an iontophoretic release source for DA; 3) verify the correctness of the algorithm by comparing results with limiting analytical solutions; and 4) simulate the behavior of DA in the neostriatum with this paradigm, both as a means to explore the implications of this nonlinear system and as a practical guide to implementing an experimental paradigm.

## THEORY AND RESULTS

### Definition of concentrations

Problems involving multiphase media require careful definition of concentration. This is particularly true here where comparisons arise between the kinetic parameters measured in classical studies on slices and homogenates using radiotracers and the parameters appearing when FCV is used.

It is worth noting the explicit assumption that continuous macroscopic equations are suitable for the discussion of this problem. Using the technique of volume averaging and appropriate theorems, this has been established for diffusion with linear uptake (Nicholson and Phillips, 1981), but here it will be assumed that this is valid for the case of nonlinear uptake as well; this implicit assumption has been made in all previous work. It is known that the structure of the striatum can lead to heterogeneity, and this may account for the spatial variability of evoked DA measurements (Garris et al., 1994a). This variation, however, extends over dimensions of more than 100 $\mu$m, whereas the typical averaging volume required by the theory has a dimension of the order of 10 $\mu$m (Nicholson and Phillips, 1981), i.e., the diameter of a carbon fiber microelectrode, so the concept of local volume averaging is likely to be valid.

Consider some small volume of tissue $v$ (dm$^3$) that is composed of an extracellular phase of volume $u_o$, an intracellular phase of volume $u_i$, and solids phase $u_s$ (the volume taken up by membranes) so that $v = u_o + u_i + u_s$. Then for some substance that distributes between the two cellular phases (assuming a negligible amount is in the solid phase) $n = n_o + n_i$, where $n$ is the amount of substance ($\mu$mol) in $v$ and $n_o$ and $n_i$ are the amounts in the extracellular and intracellular phases, respectively. Several concentrations can be defined as follows. Let $c$ ($\mu$M) be defined as total amount in $v$ divided by the total volume, then

$$c = \frac{n}{v} = \frac{n_o + n_i}{u_o + u_i + u_s} = \frac{n_o}{u_o + u_i + u_s} + \frac{n_i}{u_o + u_i + u_s} = c_o + c_i \quad (1)$$

where this defines the extracellular phase average $c_o$ and the intracellular phase average $c_i$ (the concept of phase average is defined rigorously by Gray and Lee, 1977). These averages are obtained by measuring the amount of substance in the respective phase and then dividing by the whole volume. But the "extracellular concentration" and "intracellular concentration" are actually intrinsic phase averages obtained by dividing the amount in a given phase by the volume of that phase. This can be made explicit by introducing the variables $c_o^o$ and $c_i^i$, which are defined by

$$c = \frac{u_o}{(u_o + u_i + u_s)}\frac{n_o}{u_o} + \frac{u_i}{(u_o + u_i + u_s)}\frac{n_i}{u_i} = \alpha c_o^o + \beta c_i^i. \quad (2)$$

Here the extracellular volume fraction, $\alpha = u_o/(u_o + u_i + u_s)$, and intracellular volume fraction, $\beta = u_i/(u_o + u_i + u_s)$, have been introduced. More commonly, in the literature on porous media volume fraction is denoted by $\phi$, so $\phi_o$ and $\phi_i$ would be used, but $\alpha$ and $\beta$ will be used here to maintain continuity with previous papers dealing with brain tissue. Note that the

total water content of brain tissue gray matter is about 85% (Katzman and Pappius, 1973), i.e., $\alpha + \beta = 0.85$. Assuming $\alpha = 0.2$ (Rice and Nicholson 1991), then $\beta = 0.65$ and the volume fraction of the solids, $u_s/(u_o + u_i + u_s)$, is 0.15.

## Equation for behavior of DA in extracellular space

There are many ways to derive the partial differential equation describing the relation between diffusion and uptake. Here a simple approach is taken based on the specific spherical geometry appropriate to this problem.

A spherical iontophoresis electrode of radius $r_0$ (cm) emits a flux of DA, $J_0$ ($\mu$mol cm$^{-2}$ s$^{-1}$). The real iontophoresis electrode has a radius of 1–2 $\mu$m, and the tip is a disk, because it is the cut end of a glass capillary tube. Such a boundary condition introduces unnecessary complexity without adding anything to the problem, because the detailed structure of the electrode tip plays a negligible role in the solution when measurements are made a few micrometers away, as they always are in practice. On the other hand, the point source used satisfactorily in analytical solutions to linear iontophoresis problems (e.g., Nicholson and Phillips, 1981) is inappropriate for the numerical solution to be developed here.

Consider a spherical shell at a distance $r$ from the center of the emitting electrode (Fig. 1). The thickness of the shell is $\delta r$, the areas of the inner and outer surfaces of the shell are $A(r)$, and $A(r + \delta r)$, and the fluxes on the inner and outer surfaces of the shell are $J(r)$ and $J(r + \delta r)$, respectively. Then, performing a mass balance on the flux through the volume element of the spherical shell:

$$A(r)\delta r \frac{\partial c}{\partial t} = A(r)J(r) - A(r + \delta r)J(r + \delta r) \qquad (3)$$

approximating $A(r + \delta r)$ and $J(r + \delta r)$ with Taylor expansions and neglecting terms in $\delta r^2$ and higher:

$$A(r + \delta r) \approx A(r) + \frac{\partial A}{\partial r}\delta r; \quad J(r + \delta r) \approx J(r) + \frac{\partial J}{\partial r}\delta r$$

so that Eq. 3 becomes (writing $A$ and $J$ for $A(r)$ and $J(r)$, respectively, and again neglecting terms in $\delta r^2$)

$$A \frac{\partial c}{\partial t} = -\left(A \frac{\partial J}{\partial r} + J \frac{\partial A}{\partial r}\right) = -\frac{\partial (AJ)}{\partial r}. \qquad (4)$$

The required relation between flux and concentration can be described by Fick's first law recast appropriately for a porous medium. The justification for the form used has been the subject of discussion (e.g., Aris, 1975; Nicholson and Phillips, 1981), but in essence it is necessary to recognize that the flux is driven by the extracellular concentration gradient in the interstices of the extracellular space, $\delta c_o^o/\delta r$. It is assumed that within the narrow clefts between cells, diffusion is governed by the free diffusion coefficient $D$ (cm$^2$ s$^{-1}$). The effect of the obstructed extracellular space is accounted for by a modified diffusion coefficient, $\alpha D/\lambda^2$, where $\lambda$ (non-

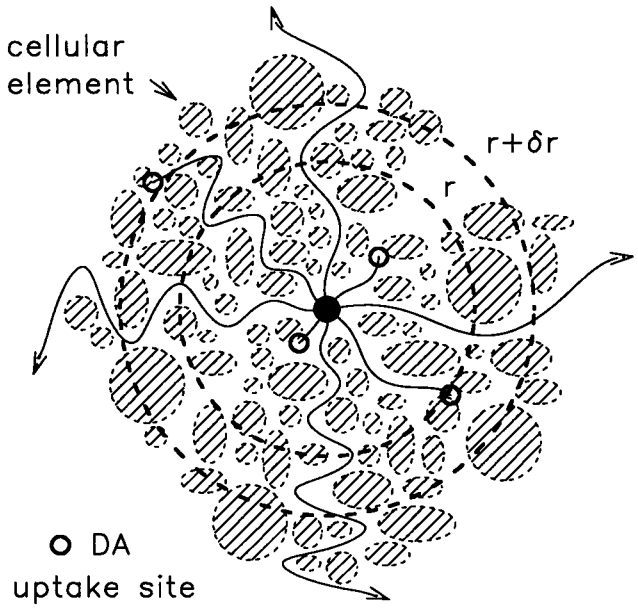


FIGURE 1 Some concepts used in this paper. The brain extracellular microenvironment consists of the spaces between cellular elements (cell bodies, fibers, dendrites, glial processes). The elements are depicted here by the broken ellipses. A microelectrode, assumed to be a small sphere and indicated by the central black circle, releases DA by iontophoresis. The DA is constrained both by the reduced volume fraction ($\alpha$) of the extracellular space relative to the whole volume and the tortuosity ($\lambda$). The tortuosity is shown here in cartoon form as the wiggling lines emanating from the source electrode. The wiggles are caused by the hindrance of the diffusing particles by the cellular elements. Diffusing molecules are captured by uptake sites (*thick open circles*) located primarily in presynaptic terminals. To develop a mass-balance of the macroscopic behavior of the diffusing DA molecules, a thin shell of thickness $\delta r$ is inscribed in the tissue at a distance $r$ from the center of the releasing electrode.

dimensional) is the tortuosity. Tortuosity is a measure of the extent to which diffusing particles are hindered by the presence of obstructions, in the form of cells or their extensions (see Nicholson and Phillips (1981) for more detail). It is also frequently convenient to define an apparent diffusion coefficient $D^* = D/\lambda^2$. Then

$$J = -\alpha D^* \frac{\partial c_o^o}{\partial r}; \quad \text{hence} \quad \frac{\partial J}{\partial r} = -\alpha D^* \frac{\partial^2 c_o^o}{\partial r^2}. \qquad (5)$$

Combining Eqs. 4 and 5 and noting that $A = 4\pi r^2$ and $\partial A/\partial r = 8\pi r$

$$\frac{\partial c}{\partial t} = \alpha D^* \left(\frac{\partial^2 c_o^o}{\partial r^2} + \frac{2}{r}\frac{\partial c_o^o}{\partial r}\right). \qquad (6)$$

It remains to define the time derivative on the left-hand side of Eq. 6. From Eqs. 1 and 2, this can be written:

$$\frac{\partial c}{\partial t} = \alpha \frac{\partial c_o^o}{\partial t} + \frac{\partial c_i}{\partial t} \qquad (7a)$$

$$\text{or} \quad \frac{\partial c}{\partial t} = \alpha \frac{\partial c_o^o}{\partial t} + \beta \frac{\partial c_i^i}{\partial t}. \qquad (7b)$$

*Michaelis-Menten kinetics*

Classical experiments that determine the Michaelis-Menten constants measure the entry into cells of a substance that has been labeled with a radioactive tracer (consequently, it does not become lost even if broken down chemically). In this way, $V_{max}$ is given as a function of tissue weight, which may be the whole tissue, in which case Eq. 7a would be valid or steps may be taken to ensure that just the intracellular mass is considered so that Eq. 7b would be appropriate. Weight can be translated to total volume assuming a density of 1 g $cm^{-3}$ for brain tissue. In other cases, $V_{max}$ is measured in terms of protein content, which may again be converted to volume by making appropriate assumptions. It is clear that $V_{max}$ is not well defined by classical experiments and that subtle differences exist in the quantities measured in different laboratories. Because it is necessary to adopt some definition that relates to the large body of existing literature, the first form of Eq. 7a will be used here, recognizing that it may be equally valid to multiply $V_{max}$ by $\beta$. In any event, because $\beta$ is approximately 0.65 (see above), the error involved in omitting the term will not be great. Fortunately, the concentration dependence of $K_m$ is not so ambiguous because experiments invariably obtain $K_m$ by bathing cells in a known extracellular concentration of substance that corresponds to $c_o^o$. In reality, in many experiments involving slices or minces, this concentration is not known accurately because of diffusional effects and uncertainties about the relative sizes of the intracellular and extracellular compartments (see Green, 1976; Mireylees et al., 1986; Near et al., 1988). But in experiments involving dispersed cells or synaptosomes, the assumption will hold and will be assumed true here. Finally, therefore, the standard form of Michaelis-Menten kinetics (Christensen, 1975; Rubinow, 1975) can be used to describe the uptake

$$\frac{\partial c_i}{\partial t} = \frac{V_{max} c_o^o}{K_m + c_o^o} \tag{8}$$

where $V_{max}$ is the maximum velocity of uptake (nmol $s^{-1}$ $g^{-1}$ or $\mu M\ s^{-1}$, where 1 g of tissue is assumed to be equivalent to 1 $cm^3$) and $K_m$ is the Michaelis-Menten constant ($\mu M$).

Among the many assumptions made in deriving Eq. 8 to describe DA uptake kinetics is the requirement that the uptake proceeds only in the forward direction; this is the classical assumption that only the initial velocity need be considered. Measurements on tissue (Snyder and Coyle, 1969; Holz and Coyle, 1974) suggest that this is valid for periods of at least 2 min.

Given Eq. 8, Eq. 7a can be written as

$$\frac{\partial c}{\partial t} = \alpha \frac{\partial c_o^o}{\partial t} + \frac{V_{max} c_o^o}{K_m + c_o^o} \tag{9}$$

Because the equations will only involve $c_o^o$, it is convenient to define $C \equiv c_o^o$, so finally, combining Eqs. 6 and 9,

$$\frac{\partial C}{\partial t} = D^* \left[ \frac{\partial^2 C}{\partial r^2} + \frac{2}{r} \frac{\partial C}{\partial r} \right] - \frac{1}{\alpha} \left[ \frac{V_{max} C}{K_m + C} \right]. \tag{10}$$

*Nondimensional variables*

It will be useful to formulate the problem in terms of nondimensional variables, following the paper by Lin (1976), which will be important later.

The outer surface of the electrode is at a distance $r_o$ from the origin, and this provides a natural measure of length to form nondimensional distances. It is useful to introduce a fixed concentration, $C_o$, that will be defined later, to form the nondimensional concentrations. nondimensional variables then can be introduced:

$$R \equiv \frac{r}{r_o}; \quad T \equiv \frac{D^* t}{r_o^2}; \quad U \equiv \frac{C}{C_o}; \tag{11}$$

and using these definitions, further nondimensional Michaelis-Menten parameters can be defined:

$$V \equiv \frac{r_o^2 V_{max}}{\alpha D^* C_o}; \quad K \equiv \frac{K_m}{C_o} \tag{12}$$

With these definitions, Eq. 10 becomes:

$$\frac{\partial U}{\partial T} = \frac{\partial^2 U}{\partial R^2} + \frac{2}{R} \frac{\partial U}{\partial R} - \frac{VU}{K + U}. \tag{13}$$

*Boundary conditions*

To define the problem, an expression is needed for the spatial derivative of $U$ over the electrode surface at $R = 1$, which is equivalent to considering the flux at $r_o$. This can be done using Eq. 5, and transforming variables to the nondimensional coordinate system and re-arranging in the form:

$$H(T) \equiv -\left. \frac{\partial U}{\partial R} \right|_{R=1} = \frac{J_o(t) r_o}{\alpha D^* C_o} \tag{14}$$

where $H$ is defined by this expression.

One way to fix the meaning of $C_o$ is by considering the simplest diffusion problem in this geometry, namely, a problem with no uptake ($V_{max} = 0$) and where the distribution has reached a steady state ($\partial C/\partial t = 0$). Eq. 10 then has the solution (using Eq. 14)

$$C = \frac{J_o r_o^2}{\alpha D^*} \frac{1}{r}. \tag{15}$$

If $C_o$ is chosen to be the value of $C$ at $r = r_o$ under these conditions, then $H = 1$.

*Iontophoresis*

When a current $I$ (amps) is applied to the iontophoresis electrode and the transport number for DA at this electrode is $n$ (nondimensional), then a source $Q(t)$ ($\mu$mol $s^{-1}$) can be defined using Faraday's electrochemical equivalent $F$ (96485.3 C $mol^{-1}$):

$$Q(t) = \frac{I(t) n}{F} \tag{16}$$

and $J_o$ can be expressed in terms of $Q$ and the surface area

of the source electrode:

$$J_o(t) = \frac{Q(t)}{4\pi r_o^2}. \tag{17}$$

In the numerical solutions that follow, a rectangular pulse of current will be used for $I(t)$, but an arbitrary function of time could serve equally well.

## Numerical solution of the diffusion equation with Michaelis-Menten uptake

Equation 10 is similar to a formulation of the mathematical problem of oxygen diffusion and consumption in tissue or cellular aggregates. As long ago as 1932, Roughton recognized that the oxygen problem led to a nonlinear equation with no analytical solutions (Roughton, 1932, 1952). Roughton simplified the problem to one of linear uptake (i.e., uptake proportional to concentration) for which analytical solutions are relatively straightforward. From the perspective of the present study, spherically symmetric problems are of primary interest, and these center on oxygen consumption by a spherical cell bathed in a constant oxygenated medium which, for the steady-state situation, leads to a two-point boundary value problem. One of first attempts at a numerical solution of this type of problem was given by Lin (1976), but it was shown by McElwain (1978), Anderson and Arthurs (1980), and Hiltmann and Lory (1983), all using different approaches, that Lin's solution had significant inaccuracies. Furthermore, only Lin's paper attempted to solve the time-dependent case.

Based on the earlier studies, Tosaka and Miyake (1982) proposed and implemented a method that relied on first converting the partial differential equation used by Lin to an integral equation and then solving that problem by standard numerical methods to yield both the steady-state and the time-dependent solution. The validity of the approach of these authors was verified by Schultz and King (1987) using the entirely different collocation method, and we have checked the validity of Tosaka and Miyake's numerics by implementing their method and reproducing their data (L. Tao, K.-W. Tsao, and C. Nicholson, unpublished data).

The present problem differs from the oxygen consumption problem studied by Tosaka and Miyake in the boundary conditions which, in turn, affect the construction of the integral equation, so it is necessary to derive the appropriate equation, following the approach of Tosaka and Miyake. For consistency, the formulation of the DA problem in nondimensional variables, given above, conforms to the conventions adopted by Lin (1976) and Tosaka and Miyake (1982).

### *Derivation of the integral equation*

Re-arranging the order of Eq. 13, multiplying throughout by $R^2$, and then integrating from 1 to $R$ results in (where $\rho$ is a variable of integration):

$$R^2\frac{\partial U}{\partial R} - \frac{\partial U}{\partial R}\bigg|_{R=1} = \int_1^R \rho^2 \frac{\partial U}{\partial T}\,d\rho + \int_1^R \rho^2 \frac{VU}{K+U}\,d\rho. \tag{18}$$

Using the boundary condition represented by Eq. 14,

$$\frac{\partial U}{\partial R} = -\frac{H(T)}{R^2} + \frac{1}{R^2}\left\{\int_1^R \rho^2 \frac{\partial U}{\partial T}\,d\rho + \int_1^R \rho^2 \frac{VU}{K+U}\,d\rho\right\}. \tag{19}$$

Integrating again between 1 and $R$ and using integration by parts on the expression in the curly brackets (see Tosaka and Miyake (1982) for details) yields:

$$U(R) = U(1) - \left(1 - \frac{1}{R}\right)H(T) - \frac{1}{R}\int_1^R \rho^2\left(\frac{\partial U}{\partial T} + \frac{VU}{K+U}\right)d\rho + \int_1^R \rho\left(\frac{\partial U}{\partial T} + \frac{VU}{K+U}\right)d\rho. \tag{20}$$

Note that, in contrast with the problem of oxygen diffusion into a cell (Tosaka and Miyake, 1982), it is not necessary to consider the potential singularity at $R = 0$ because the point is excluded in this problem. It is required, however, to evaluate $U(1)$. To do this, let $R \to \infty$ and assume that:

$$\lim_{R\to\infty} U(R) = 0 \text{ and } \lim_{R\to\infty} \frac{1}{R}\int_1^R \rho^2\left(\frac{\partial U}{\partial T} + \frac{VU}{K+U}\right)d\rho = 0. \tag{21}$$

Then

$$U(1) = H(T) - \int_1^\infty \rho\left(\frac{\partial U}{\partial T} + \frac{VU}{K+U}\right)d\rho. \tag{22}$$

Inserting Eq. 22 into Eq. 20 finally yields:

$$U(R) = \frac{H(T)}{R} - \frac{1}{R}\int_1^R \rho^2\left(\frac{\partial U}{\partial T} + \frac{VU}{K+U}\right)d\rho - \int_R^\infty \rho\left(\frac{\partial U}{\partial T} + \frac{VU}{K+U}\right)d\rho. \tag{23}$$

### *Implementation of solution*

The following is based on the numerical approach of Tosaka and Miyake (1982) and is only outlined here. The scheme for the solution consisted of three procedures: 1) generation of a set of nonlinear algebraic equations by approximating the time derivative and integrals by discrete formulations; 2) solution of the equations by an iterative nonlinear equation solver; and 3) inversion of the resulting linear matrices by an appropriate numerical method.

The time derivatives in Eq. 23 were approximated by introducing a small time increment, $\Delta T$ and writing the forward finite difference scheme:

$$\frac{\partial U}{\partial T} \cong \frac{U(R, T + \Delta T) - U(R, T)}{\Delta T}. \quad (24)$$

The interval [0, ∞] was replaced by [0, $R_\infty$], where $R_\infty$ is a suitably large number and the interval divided into $m$ subintervals. The integrals were then approximated by the trapezoidal rule (Press et al., 1986), and a set of $m + 1$ nonlinear equations generated at each discrete time increment.

This set of nonlinear equations was solved by the Newton-Raphson method (Press et al., 1986) which, in turn, required the solution of a set of linear algebraic equations. This final step was accomplished efficiently using the LU decomposition method (Press et al., 1986).

In applying the Newton-Raphson, algorithm it was found necessary: 1) to test for the emergence of small negative concentrations ($U < 0$) throughout the calculation and, if they occurred, set the concentration at that point on that time step equal to zero; and 2) to explicitly derive and implement the limiting forms of $VU/(K + U)$ and its derivative for the conditions $U > 100K$ or $U < 0.01K$.

### *Parameters for numerical calculations*

A value of $D = 6.9 \times 10^{-6}$ cm$^2$ s$^{-1}$ was used for the diffusion coefficient of DA. This was based on the value of $D$ at 25°C (Gerhardt and Adams, 1982) corrected to 32°C (the temperature typically used for brain slices), assuming the temperature dependence was 2% per degree. Volume fraction ($\alpha$) was taken as 0.21, and tortuosity ($\lambda$) was taken to be 1.54 (Rice and Nicholson, 1991). This tortuosity means that the apparent diffusion coefficient, $D^*$, is 2.37 times smaller than $D$. A transport number of $n = 0.01$ was used for the source electrode (Rice and Nicholson, 1989). The duration of the iontophoresis was either infinite (steady-state calculations) or 10 s. Other parameters were varied to address different issues and are described in the text and figures, but usually the radius of the source electrode, $r_0$, was 2 μm and the source current was $I = 100$ nA (although this was varied in several instances). For the reasons described below, $K_m$ was often 0.15 or 6.0 μM and $V_{max}$ was 0.2 or 0.8 μM s$^{-1}$. When concentration versus time curves were calculated, the typical separation between source and recording position was $r = 100$ μm.

In the numerical methods, $r_\infty$ was often 400 μm, but increased when appropriate. The interval from $r_0$ to $r_\infty$ was usually divided into 240 subintervals. In time-dependent calculations, a time step of 0.125 s was used. These numerical calculation parameters were varied to establish that they did not compromise the calculations.

The numerical solution was implemented in Pascal (Borland Turbo Pascal v. 7.0) using the algorithms described in the above-mentioned chapters by Press et al. With the mesh and step sizes defined above, a typical calculation took about 2 h on a PC equipped with a 60 MHz Pentium microprocessor.

## Steady-state solution: comparison with analytic approximations

The following section will compare analytical approximations to the steady-state solutions for the diffusion equation with the numerical solutions. This both enables the accuracy of the numerics to be checked and provides insight into the behavior of this nonlinear equation. The final part of the paper will use these insights to discuss the time-dependent solution. Before commencing, it will be necessary to have specific values for the uptake parameters.

### *Established values of the Michaelis-Menten parameters*

Values for $V_{max}$ and $K_m$ have been obtained from preparations of homogenates, synaptosomes, or slices using [$^3$H]DA; some representative values are given in Table 1. To make sense of the different estimates from the literature it is necessary to convert the various units for "$V_{max}$" into a standard form, and the units of μM s$^{-1}$ have been chosen using

**TABLE 1 Some Michaelis-Menten parameters for striatum**

| Species | Preparation | "$V_{max}$" | "$V_{max}$" units | $V_{max}$ μM s$^{-1}$ | $K_m$ μM | Ref. |
|---|---|---|---|---|---|---|
| Rat | Homogenates | 100 | nmol (g pellet)$^{-1}$ (5 min)$^{-1}$ | 0.33 | 0.4 | (1) |
| Rat | Slices | 4.08–5.00 | nmol (g tissue)$^{-1}$ min$^{-1}$ | 0.08* | 0.33–0.40* | (2) |
| Rat | Synaptosomes | 25.3 | pmol (100 μg protein)$^{-1}$ (2 min)$^{-1}$ | 0.21 | 0.13 | (3) |
| Rat | Synaptosomes | 106 | (mg protein)$^{-1}$ min$^{-1}$ | 0.18 | 0.14 | (4) |
| Mouse | Synaptosomes | 7.0 | nmol (g tissue)$^{-1}$ min$^{-1}$ | 0.12 | 0.21 | (5) |
| Mouse | Homogenates | 90.8 | pmol, (mg protein)$^{-1}$ min$^{-1}$ | 0.15 | 0.20 | (6) |
| Rat | In vivo | 4 | μM s$^{-1}$ | 0.84 | | (7) |
| Rat | In vivo | 4 | μM s$^{-1}$ | 0.84‡ | 6.0‡ | (7) |

"$V_{max}$" and "$V_{max}$" units refer to the quantities quoted in the original references. $V_{max}$ is the unit defined in this paper. To convert the measurements based on protein content to μM, a value of 0.1 mg protein per mg tissue (Justice, 1988, Table 1, footnote 2, of that paper) was assumed and that 1 g of tissue occupied 1 ml of volume (i.e., it is mainly water).

References cited: (1) Snyder and Coyle, 1969; (2) Shaskan and Snyder, 1970; (3) Holz and Coyle, 1974; (4) Schoemaker and Nickolson, 1983; (5) Ross, 1991; (6) Zimányi et al., 1989; (7) Wightman and Zimmerman, 1990.

*Average values for high affinity system (Uptake 1).

‡After administration of 20 mg kg$^{-1}$ nomifensine.

the definition given earlier. The conversions are shown in Table 1 along with the $K_m$ values in $\mu$M.

Wightman and co-workers have used a completely different approach to the earlier classical studies that is much more closely related to our studies. They determined $V_{max}$ in the intact anesthetized rat striatum using repetitive stimulation of the median forebrain bundle and FCV combined with carbon fiber microelectrodes. A range of values was obtained, but a typical estimate would be 4 $\mu$M $s^{-1}$ for "$V_{max}$" (Wightman and Zimmerman, 1990). In fact, this value is actually $V_{max}/\alpha$ according to the definition used in this paper, so that $V_{max}$ = 0.84 $\mu$M $s^{-1}$. These investigators could not estimate $K_m$ with their methods under normal conditions (but with improved techniques, a value of $K_m$ = 0.16 $\mu$M was obtained recently in the striatum by Garris and Wightman, 1994b). In the presence of the DA uptake blocker nomifensine, Wightman and co-workers (Wightman and Zimmerman, 1990) saw $K_m$ rise to the measurable value of about 6 $\mu$M without a significant change in $V_{max}$.

It is evident from Table 1 that there is considerable consistency among the synaptosome, homogenate, and intact tissue determinations of $V_{max}$ and $K_m$ but that the value of $V_{max}$ obtained with FCV is about 4 times higher (range 1–8 times). This discrepancy is not very large, but for the purposes of exploring the solutions of the equations presented here, two standard values for $V_{max}$ will be used, based on data from rat striatum, of 0.2 and 0.8 $\mu$M $s^{-1}$ and a single value for $K_m$ of 0.15 $\mu$M.

### *The free boundary case ($U \gg K$)*

When the nondimensional concentration $U$ is much greater than $K$ (i.e., $C \gg K_m$), then the uptake term will approach a constant, $V$. This appears to be a simple case, but it is not and belongs to a class of interesting and complex problems known as moving-boundary problems (Crank, 1984) with only a few, specialized, analytical solutions. In the present paper, one of the simplest solutions for the steady-state distribution is derived; however, this example will provide insight into the nature of nonlinear uptake and a test of the numerics.

The problem is formulated as steady release of DA from a spherical electrode into a medium characterized (in nondimensional variables) by a constant uptake $V$ (here $K_m = 0$ so that $C \gg K_m$ for most $C$). Intuitively, it is clear that there must be a boundary at a distance $B = b/r_o$ from the center of the electrode beyond which there is no DA. This boundary cannot be specified without solving the diffusion problem, however. Because this boundary does not move in the steady-state case, this problem is referred to as a free-boundary problem (Crank, 1984).

It is necessary to solve the following equation (from Eq. 13):

$$\frac{1}{R^2}\frac{d}{dR}\left(R^2\frac{dU}{dR}\right) - V = 0 \qquad (25)$$

subject to two conditions on the free boundary:

$$U = 0 \quad \text{and} \quad \frac{dU}{dR} = 0 \quad \text{at} \quad R = B. \qquad (26)$$

The first condition is obvious, and the second is a characteristic condition imposed on free-boundary problems (Crank, 1984). Integrating Eq. 25 twice and using conditions (26), one obtains (c.f. Appendix 1 of Chaplain and Stuart, 1991)

$$U = \frac{V}{6}\left[R^2 + 2\frac{B^3}{R} - 3B^2\right]. \qquad (27)$$

Finally, an explicit value for $B$ is derived by using the boundary condition represented by Eq. 14, and this yields

$$B = \left[1 + 3\frac{H}{V}\right]^{1/3}. \qquad (28)$$

When translated back into the real coordinate system using Eqs. 11, 12, 14, and 17 the expression becomes

$$b = \left[r_o^3 + \frac{3Q}{4\pi V_{max}}\right]^{1/3}. \qquad (29)$$

Interestingly, if $V_o$ is defined to be the volume occupied by the spherical electrode and $V_{DA}$ to be the volume where DA is to be found, then

$$V_{DA} = V_o + \frac{Q}{V_{max}}. \qquad (30)$$

A consequence of Eqs. 29 and 30 is that the boundary of the territory invaded by the DA is only defined by the source magnitude, the size of the iontophoresis electrode and $V_{max}$. In fact, the size of the electrode can almost always be neglected for typical parameters used here.

An important and nonintuitive consequence of Eqs. 29 and 30 is that the location of the boundary does not depend on the diffusion properties of the medium. The amplitude of the spatial distribution does depend on these properties, however. Translating Eq. 27 into dimensional variables results in

$$C = \frac{1}{\alpha D^*}\frac{V_{max}}{6}\left[r^2 + 2\frac{b^3}{r} - 3b^2\right]. \qquad (31)$$

To assess how closely the analytical solution, Eq. 31, based on $C \gg K_m$, approximates the actual steady-state solution obtained by numerical solution for all values of $C$, three sets of curves are plotted in Fig. 2. All of the curves are for $I$ = 100 nA with $n$ = 0.01, and the two standard values of $V_{max}$ are used. For the numerical calculation, two solutions are obtained, the first with $K_m$ = 0.15 $\mu$M, the standard value, and the second with $K_m$ = 6 $\mu$M, the value obtained in the presence of nomifensine. It is seen that for both sets of $K_m$ values, the analytic solution does indeed fit the full numerical solution well for $C \geq 10K_m$ (i.e., $C \geq$ 1.5 $\mu$M and $C \geq$ 60 $\mu$M, respectively). It is also evident that the drastic increase in $K_m$ causes the DA to extend much further from the source.

It is worth explicitly noting that a defined boundary at $r = b$ apparently only strictly exists in the case $K_m = 0$; when

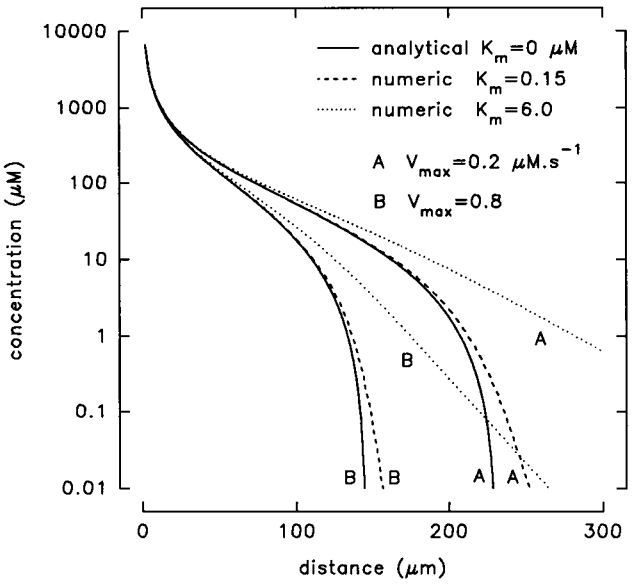


FIGURE 2 Comparison of analytical steady-state solution (i.e., current applied for infinite time) for $K_m = 0$ with complete numerical solution with two values of $K_m$. In this figure, the ordinate is scaled logarithmically. The solid line represents the analytical solution represented by Eq. 31 for $I$ = 100 nA and the two values of $V_{max}$, 0.2 μM s$^{-1}$ ($A$) and 0.8 μM s$^{-1}$ ($B$). These solutions are computed under the assumption that $K_m = 0$, hence, $C \gg K_m$. The dashed lines show solutions for two realistic values of $K_m$, 0.15 μM (normal value in rat striatum) and 6.0 μM (value in presence of nomifensine). These solutions were obtained by numerical solution of Eq. 23, as detailed in the text, for the time-independent case. It is seen that the normal value of $K_m$ results in a steady-state solution that is quite close to the analytical approximation when $C > 10K_m$ for both values of $V_{max}$. This is also true of the value of $K_m$ appropriate for nomifensine, but in this case 10 $K_m$ = 60 μM so that the analytical and numerical solutions diverge over most of the range of values shown. Unless otherwise stated, all calculations in this and subsequent figures use these *standard parameters*: $D = 6.9 \times 10^{-6}$ cm$^2$ s$^{-1}$, $\alpha = 0.21$, $\lambda = 1.54$, $r_o = 2$ μm, $n = 0.01$.

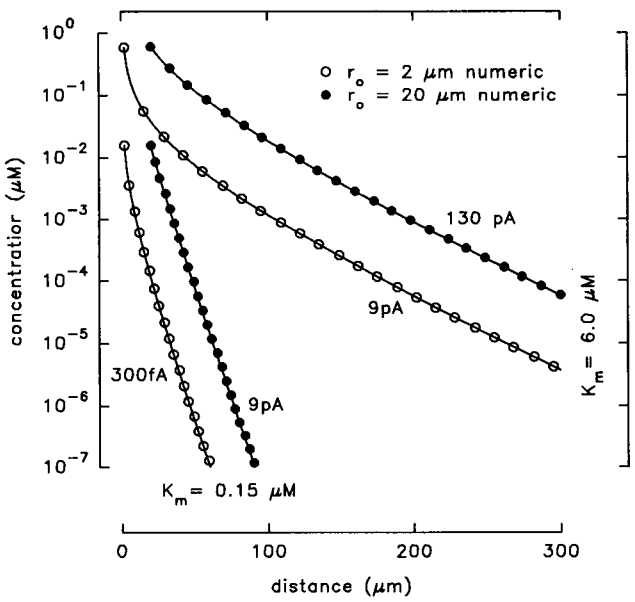


FIGURE 3 Comparison of analytical and numerical steady-state solutions (i.e., current applied for infinite time) for $C \ll K_m$. In all cases, $V_{max}$ = 0.2 μM s$^{-1}$. Based on the criterion that the two solutions should agree for $C \leq K_m/10$, the maximum currents needed to satisfy this criterion for two different radii of the source electrode were calculated from Eq. 47 (see text). For the standard radius ($r_o$ = 2 μm) of the source electrode, numerical solutions were computed (○) and compared with the analytical solution given by Eq. 44 for $I$ = 300 fA and $K_m$ = 0.15 μM and $I$ = 9 pA and $K_m$ = 6 μM. To assess the influence of the size of the stimulating electrode, the comparison was repeated for a source electrode with $r_o$ = 20 μm (●) for $I$ = 9 pA and $K_m$ = 0.15 μM and $I$ = 130 pA and $K_m$ = 6 μM. In all cases, the analytical and numerical solutions were indistinguishable. Note the range of the ordinate in the figure differs from that in Fig. 2. See legend to Fig. 2 for standard parameters.

$K_m > 0$, the boundary "creeps" forward as lower and lower concentrations are examined. This seen in Fig. 2 (and is even better shown in Fig. 4) for the numerical solutions with finite $K_m$. In practice, of course, when concentrations fall below some small value they can can neither be detected nor activate receptors.

### *The linear uptake case ($K \gg U$)*

Here the uptake limit is (defining $W = V/K$):

$$\lim_{K \gg U} \frac{VU}{K + U} \rightarrow \frac{V}{K} U = WU. \tag{32}$$

It follows that $W$ can be defined in terms of the original parameters as:

$$W = \frac{r_o^2}{\alpha D^*} \frac{V_{max}}{K_m}. \tag{33}$$

The time-dependent problem, represented by Eq. 13, now can be solved analytically, and the complete solution is given below, although only the steady-state result will be used in this section.

Because the point $R = 0$ is excluded from this problem, a new variable $P$ can be defined such that $U = PR^{-1}$ (where both $U$ and $P$ are functions of $R$ and $T$), and then Eq. 13 becomes:

$$\frac{\partial P}{\partial T} = \frac{\partial^2 P}{\partial R^2} - WP. \tag{34}$$

whereas the boundary condition represented by Eq. 14 is now:

$$\left(P - \frac{\partial P}{\partial R}\right)\Bigg|_{R=1} = \mathrm{H(T)}. \tag{35}$$

Equation 34 can be solved by standard techniques using the Laplace transform method. Define $s$ as the transform of the time variable $T$, and $P^*$ as the transform of $P$. Then, denoting the Laplace transform by $L$, this can be expressed formally as $L\{P(T)\} = P^*(s)$; $L^{-1}\{P^*(s)\} = P(T)$.

Then, assuming that $P(R, 0+) = 0$, Eq. 34 becomes:

$$\frac{\mathrm{d}^2 P^*}{\mathrm{d}R^2} = -(s + W)P^*. \tag{36}$$

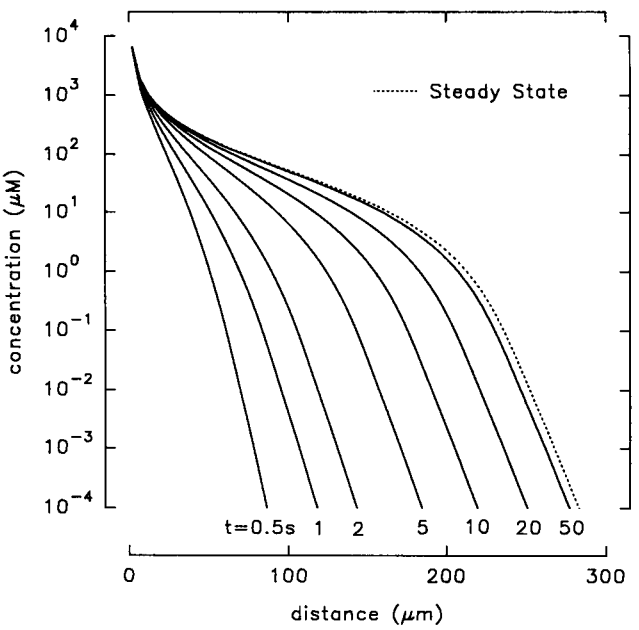


FIGURE 4 Approach to the steady-state concentration distribution. The concentration versus distance profiles are shown at 0.5, 1, 2, 5, 10, 20, and 50 s (——) together with the steady-state distribution (· · · · ·). All curves are calculated with the standard parameters given in Fig. 2 and the values $V_{max}$ = 0.2 μM $s^{-1}$, $K_m$ = 0.15 μM, $I$ = 100 nA. Note that by 50 s the distribution is close to the final steady state.

For the boundary condition at $R = 1$, the function $H(T)$ can be taken as a step function at $T = 0$ from zero to a value $H_o$; then Eq. 35 becomes:

$$\left(P^* - \frac{dP^*}{dR}\right)\bigg|_{R=1} = \frac{H_o}{s}. \tag{37}$$

Equation 36 admits of an exponential solution, and it is assumed that $P^*$ decays with distance. Incorporating the boundary condition represented by Eq. 37, one obtains the solution:

$$P^* = \frac{H_o}{s(1 + \sqrt{s + W})}\exp(-\sqrt{s + W}(R - 1)). \tag{38}$$

Using the property that

$$L\{\exp(-aT)F(T)\} = F^*(s + a)$$

where $a$ is any constant and $F$ is a function with Laplace transform $F^*$ (Carslaw and Jaeger, 1959); then

$$U = \frac{P}{R} = \frac{H_o \exp(-WT)}{R} L^{-1}\left\{\frac{\exp(-(R - 1)\sqrt{s})}{(s - W)(1 + \sqrt{s})}\right\}. \tag{39}$$

The inverse Laplace transform can be found immediately from Transform 31, Appendix V of Carslaw and Jaeger (1959) (subject to the condition that $W \neq 1$) and defining $G = (R - 1)/2\sqrt{T}$, to yield:

$$U = \frac{H_o}{R}\left[\frac{e^{-(R-1)\sqrt{W}}\operatorname{erfc}(G - \sqrt{WT})}{2(1 + \sqrt{W})} + \frac{e^{(R-1)\sqrt{W}}\operatorname{erfc}(G + \sqrt{WT})}{2(1 - \sqrt{W})} - \frac{e^{(R-1)+T(1-W)}\operatorname{erfc}(G + \sqrt{T})}{(1 - W)}\right]. \tag{40}$$

This solution can be generalized to a pulse of duration $T_P$ by linear superposition:

$$U = U(H_o, R, T) \quad \text{when} \quad T \leq T_P;\ U = U(H_o, R, T) - U(H_o, R, T - T_P) \quad \text{when} \quad T > T_P. \tag{41}$$

where $U(H_o, R, T)$ is the function given by Eq. 40.

Apart from being useful in the context of this paper, the solution given by Eqs. 40 and 41 can be applied to the analysis of data from experiments using the TMA-method to determine the diffusion characteristics of brain tissue (Nicholson and Phillips, 1981; Nicholson, 1992). Until now, that method was based on solutions involving point sources; the solution given here enables the effect of a finite source diameter to be assessed.

### *Steady-state solution*

In the limiting case as $T \to \infty$, Eq. 40 has the form (which can also be derived directly by solving the time-independent version of Eq. 34):

$$\lim_{T\to\infty} U = \frac{H_o}{R(1 + \sqrt{W})}\exp(-\sqrt{W}(R - 1)). \tag{42}$$

Define

$$\kappa = \sqrt{\alpha D^* \frac{K_m}{V_{max}}}. \tag{43}$$

Then

$$C = \frac{J_o r_o^2}{\alpha D^* r}\frac{1}{(1 + r_o/\kappa)}\exp(-(r - r_o)/\kappa) \tag{44}$$

As the spherical electrode tends to zero radius, one obtains (recalling Eq. 17):

$$\lim_{r_o\to 0}(J_o r_o^2) = \frac{Q}{4\pi} \quad \text{and} \quad C = \frac{Q}{4\pi\alpha D^* r}\exp(-r/\kappa). \tag{45}$$

This agrees with the expression derived by Nicholson and Phillips (1981) when the $k'$ of that paper is identified as follows (see also Nicholson, 1992):

$$k' = \frac{\langle S\rangle P_E}{\alpha} = \frac{k}{\alpha} = \frac{V_{max}}{\alpha K_m} = \frac{D^*}{\kappa^2}. \tag{46}$$

where $\langle S\rangle$ ($cm^{-1}$) is the volume average of the cell surface

contained in an averaging volume (also termed a representative elementary volume) and $P_E$ is the average permeability of the membrane (cm $s^{-1}$).

Equations 40, 41, 44, and 45 are only valid as solutions to Eq. 10 so long as $C \ll K_m$. (Note that these solutions are entirely valid for all values of $C$ when the uptake term in Eq. 10 is written as $k'C$, but this is not Michaelis-Menten kinetics.) One can estimate the maximum current, $I_{max}$, for which this would be valid by noting that the maximum concentration occurs at the surface of the spherical electrode ($r = r_o$) and demanding that $C(r_o) \leq K_m/10$. From Eqs. 17 and 44, this leads to an expression for $I_{max}$:

$$I_{max} = \frac{4\pi F}{n} \alpha D^* r_o \left(1 + \frac{r_o}{\kappa}\right) \frac{K_m}{10}. \quad (47)$$

Using Eq. 47 with the two standard values of $V_{max}$ (0.2 and 0.8 $\mu M\ s^{-1}$) and a $K_m$ of 0.15 $\mu M$, one obtains 290 and 350 fA, respectively. Taking a $K_m$ of 6 $\mu M$, one obtains 9.3 and 9.7 pA, respectively. Of course, these values depend on the current density at the surface of the spherical electrode, and this must decrease with increasing radius. In the calculation above, the standard value $r_o = 2$ $\mu m$ was used. Using $r_o =$ 20 $\mu m$, one obtains values of 8.8 and 15 pA for the two standard values of $V_{max}$ (0.2 and 0.8 $\mu M\ s^{-1}$) and a $K_m$ of 0.15 $\mu M$ and 130 and 170 pA for a $K_m$ of 6 $\mu M$. It is evident that (see Fig. 3), for the small concentrations generated by these low currents, the analytical solution and numerical solution are identical, as predicted above.

It is important to note that for Eq. 44 to be correct $C \ll K_m$ for all distances. In all problems for sufficiently large distances, the condition is satisfied but, because of the nonlinearity of the diffusion equation with Michaelis-Menten uptake, Eq. 44 does not predict the concentration correctly if the concentration distribution has evolved through a phase, in this case a sequence of locations, where the condition $C \ll K_m$ is violated. A corollary of this is that even if the distribution can be fitted with Eq. 44 with a suitable $\kappa$ (or $k$ or $k'$ which amount to the same thing), such a constant can only be interpreted in terms of $V_{max}$ and $K_m$ if $C \ll K_m$ holds throughout the concentration domain.

## Time-dependent solution

In general, the study of the time-dependent solution requires a full numerical calculation. The only exception is the solution when $C \ll K_m$ for all times and distances. In this situation, Eqs. 40 and 41 are valid. Practically, this involves the constraints on the current discussed at the end of the last section.

### *Approach to the steady-state solution*

The first problem of interest is to ask how rapidly the steady-state solution is achieved. Fig. 4 shows a succession of profiles for a sustained current of $I = 100$ nA at different times ranging from 0.5 to 50 s. It is evident that by 50 s (of continuous iontophoresis) the distribution is close to a steady state, i.e., that the diffusion process and the uptake process are close to balance. In the concentration versus time curves presented later, the iontophoresis only lasts for 10 s so that a steady state is not attained. In fact, after the termination of the iontophoretic current, the concentration profile will retreat back to the source; this behavior will be illustrated in later three-dimensional graphs.

It is also seen in Fig. 4 that even after only half a second, levels of DA potentially detectable by FCV could be measured 50 $\mu m$ from the source. In fact, for instantaneous release of DA at the origin (i.e., a delta function), in the absence of uptake under a pure diffusion regime, the peak of the DA distribution as a function of time can be calculated from the well known expression: $r_{max} = (6D^*t)^{1/2}$ (Berg, 1993) which, with the parameters used here, yields $r_{max} = 30$ $\mu m$, so that the distribution shown in Fig. 4 at 0.5 s is reasonable.

### *Full time-dependent solution*

In preliminary experiments (M. E. Rice and C. Nicholson, unpublished data), the typical iontophoretic duration was 10 s; thus, the distribution of DA does not reach a steady state within the vast bulk of the tissue invaded by the DA, and a full numerical solution is required. The reason for choosing this iontophoresis duration was that in actual experiments it was important to limit the exposure of the tissue to DA so as to maintain the conditions under which the equations are valid (i.e., a unidirectional reaction).

The numerical results are first displayed in Fig. 5 as a sequence of concentration versus time profiles such as would be recorded in an experiment using FCV. In this figure, except for the cases where $V_{max} = 0$, i.e., "no uptake," the panels in the left-hand column (*a–c*) depict results with $V_{max} = 0.2$ $\mu M\ s^{-1}$, whereas those in the right-hand column (*d–f*) depict results for $V_{max} = 0.8$ $\mu M\ s^{-1}$. In each panel, three results are shown: for Michaelis-Menten uptake ($K_m = 0.15$ $\mu M$), uptake suppressed with nomifensine ($K_m = 6$ $\mu M$), and the hypothetical case of zero uptake ($V_{max} = 0$). Results are shown at distances of 50, 100, and 200 $\mu m$ from the source electrode, which has the usual radius of 2 $\mu m$.

At 50 $\mu m$ from the source electrode, the three curves are fairly similar; in particular, the initial rising phase is identical, but the peak amplitudes are reduced moderately by the uptake. Nomifensine has little effect because $K_m$ is not playing much of a role. It can be said that the behavior of DA is still dominated by the proximity to the source electrode for these combinations of parameters, and the high local concentration of DA ensures that the uptake process is rapidly overwhelmed.

At 100 $\mu m$ from the source, clear-cut differences in the DA profiles are apparent. The Michaelis-Menten curve is quite triangular with the rising phase being faster than the falling for $V_{max} = 0.2$ $\mu M\ s^{-1}$ (*b*), with the converse being true for $V_{max} = 0.8$ $\mu M\ s^{-1}$ (*e*). There is now a clear distinction between the Michaelis-Menten curve and the curve derived under the action of nomifensine. Furthermore, both

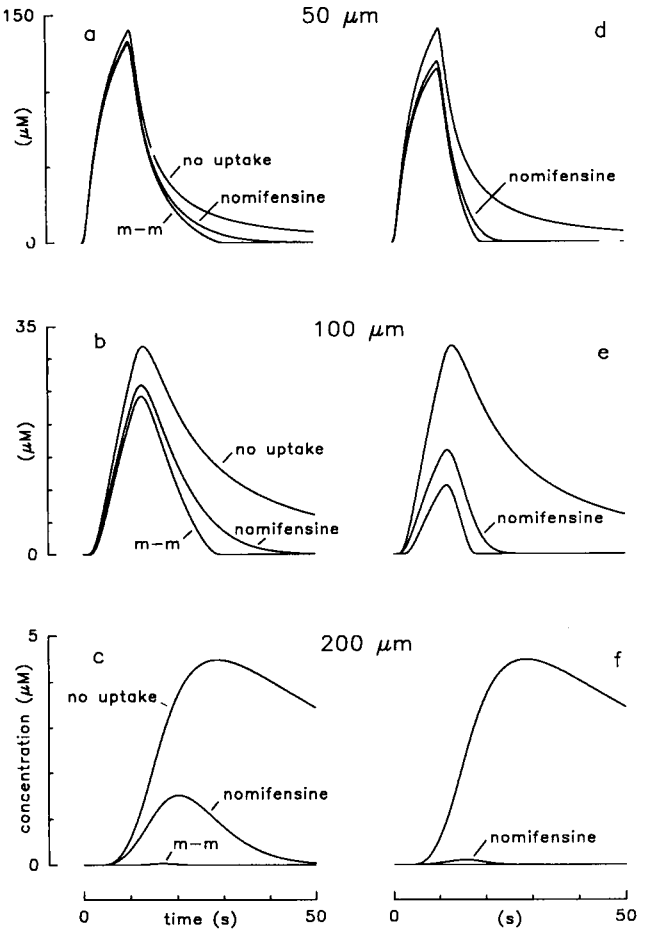


FIGURE 5 Concentration versus time curves for different distances and uptake conditions. An iontophoresis current, $I$ = 100 nA, was applied for a duration of 10 s. Each panel depicts three curves. The ones labeled "m-m" were calculated with normal Michaelis-Menten parameters $K_m$ = 0.15 μM and either $V_{max}$ = 0.2 μM $s^{-1}$ (Panels *a, b, c*) or $V_{max}$ = 0.8 μM $s^{-1}$ (Panels *d, e, f*). The ones labeled "nomifensine" were calculated with $K_m$ = 6.0 μM and either $V_{max}$ = 0.2 μM $s^{-1}$ (Panels *a, b, c*) or $V_{max}$ = 0.8 μM $s^{-1}$ (Panels *d, e, f*). The ones labeled "no-uptake" were calculated with $V_{max}$ = 0 (so $K_m$ is irrelevant). Each pair of calculations were made at three different distances from the source electrode: 50 μm (panels *a, d*), 100 μm (panels *b, e*) and 200 μm (panels *c, f*). All calculations are based on a numerical solution of Eq. 23 as described in the text. Both ordinate and abscissa are scaled linearly. See legend to Fig. 2 for standard parameters.

curves with nonlinear uptake are well differentiated from the curve without uptake.

Finally, when the distance is 200 μm from the source, the distinctions between the curves are so overwhelming that the Michaelis-Menten curves cannot even be displayed on the same scale as the curve for diffusion without uptake.

### *Effect of current on concentration distribution*

To explore further the consequences of nonlinear behavior of DA, it is convenient to adopt a different representation, in the form of a three-dimensional graph. Fig. 6 shows examples for iontophoresis currents of $I$ = 100, 10, and 1 nA. The upper graph shows data already depicted in Fig. 5 for $V_{max}$ = 0.2 μM $s^{-1}$.

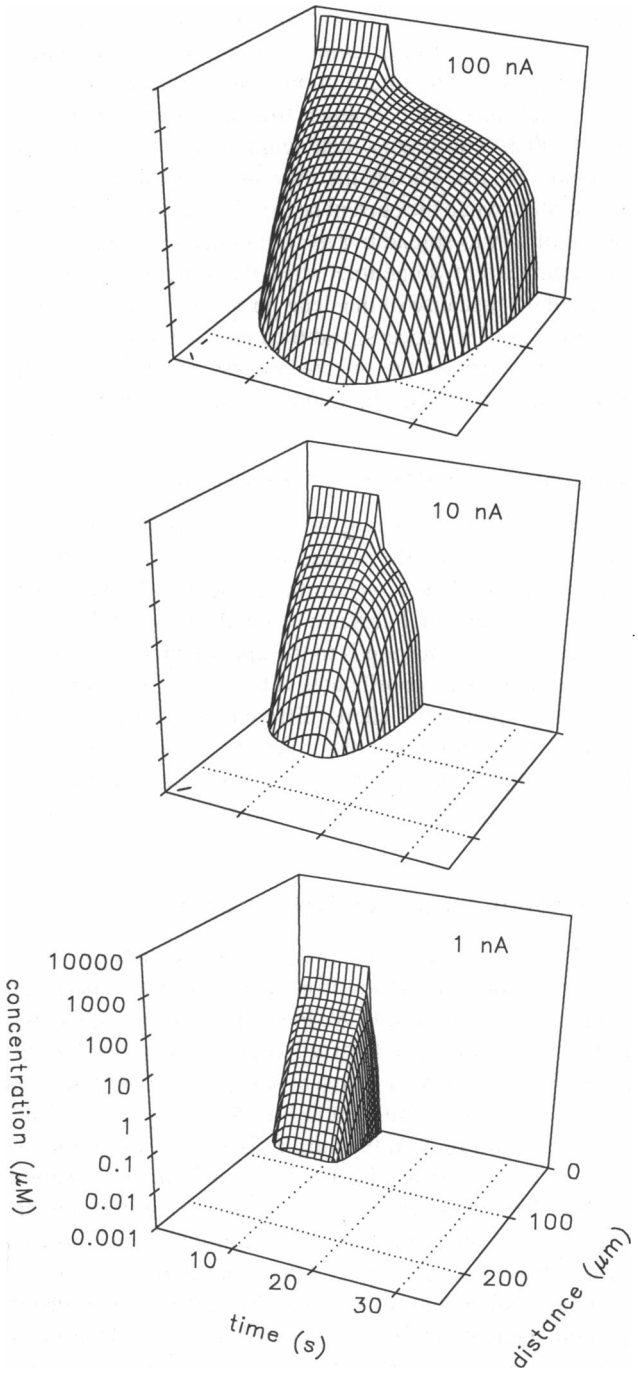


FIGURE 6 Three-dimensional plots of concentration as function of distance and time for three different iontophoresis source-current strengths applied for 10 s. These graphs illustrate the nonlinear behavior of diffusion coupled to uptake where the concentration distribution does not scale with magnitude of the source. All calculations are based on a numerical solution of Eq. 23 and use $V_{max}$ = 0.2 μM $s^{-1}$, $K_m$ = 0.15 μM. The upper graph was computed with $I$ = 100 nA, the middle graph with $I$ = 10 nA, and the bottom graph with $I$ = 1 nA. The graphs were computed as a set of concentration versus distance curves (240 points) at selected times (15–30 instances) and the surface-mesh points selected and interpolated using the graphing program SigmaPlot 5.0, (Jandel Scientific). See legend to Fig. 2 for standard parameters.

What Fig. 6 shows is that the spatio-temporal distribution of DA changes its shape as the current diminishes, in particular, how the DA surface shrinks ever closer to the source electrode as the current diminishes and the 1 nM contour, which represents the intersection of this concentration with the time-distance plane, changes from a roughly circular contour at 100 nA current to a rectangular one at 1 nA, extending to about 100 $\mu$m during the current but vanishing almost immediately when the current ceases. The general trend is for a wave of DA to spread out to certain distance, reaching its maximum extent sometime after the time the current is switched off, because of the delay produced by the diffusion component of the process, and then recede back to the electrode and vanish as the uptake process removes all of the released material from the extracellular compartment.

### *Comparison of the different uptake paradigms*

The three-dimensional representation is used in Fig. 7 to dramatically show the differences between Michaelis-Menten uptake alone (*top*), in the presence of nomifensine (*middle*), and the total absence of uptake (*lower*). Note that the upper panel corresponds to the upper panel of Fig. 6, but the time and space coordinates differ. The logarithmic ordinate accentuates the shape differences and clearly demonstrates that nonlinear uptake acts to confine DA in both space and time, whereas pure diffusion allows particles to invade the entire spatio-temporal domain.

## Implications for the analysis of data

A major goal of this paper is to provide a strategy for extracting kinetic information from an experimental paradigm using iontophoresis and FCV. In such experiments, DA will be detected at a carbon fiber microelectrode about 100 $\mu$m distant from the source of current strength $I = 100$ nA. Some typical records are simulated in Fig. 8 using $V_{max} = 0.2$ and 0.8 $\mu$M s$^{-1}$. In Fig. 8 *A*, the current is 100 nA using the two values of $V_{max}$, whereas Fig. 8 *B* shows the influence of nomifensine. The major effect of the uptake inhibitor at this distance is to enhance somewhat the amplitude and to slow the falling phase, particularly as it approaches the baseline.

An interesting contrast with the above data is provided by reducing the iontophoresis current of the source electrode by a factor of five, to $I = 20$ nA (Fig. 8 *C*). At the same distance, the DA signal is now greatly reduced (compared with panel *A*) for $V_{max} = 0.2$ $\mu$M s$^{-1}$ and the signal for $V_{max} = 0.8$ $\mu$M s$^{-1}$ is effectively zero (although as the *inset* shows, it does reach a level of a few nM). This is accompanied by a significant sharpening of the waveform, most evident in the falling phase. For this lower current, the effect of nomifensine is dramatic both in its increase in the size of the waveform and its effect on the shape, particularly for the higher value of $V_{max}$ (Fig. 8 *D*).

The implications of these data are that very subtle shape changes are involved in distinguishing the different cases. Practically, the goal is to determine $V_{max}$ in the normal brain,

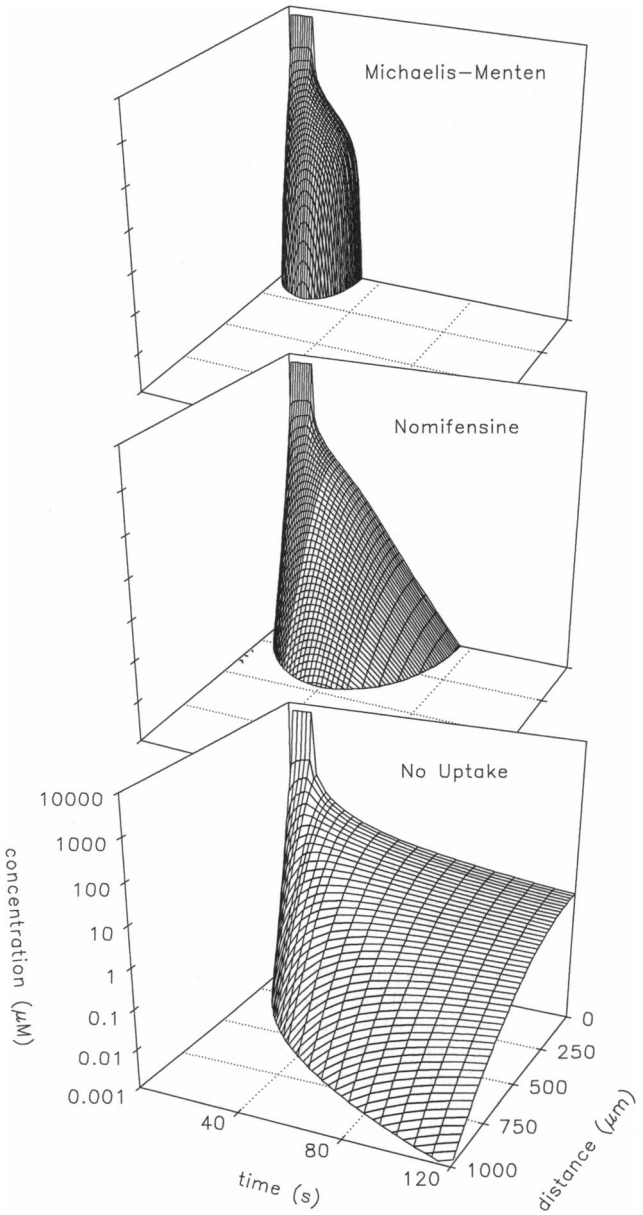


FIGURE 7 Three-dimensional plots of concentration as function of distance and time for three different uptake conditions. All calculations were based on a numerical solution of Eq. 23 and $I = 100$ nA and was applied for 10 s. The upper graph was computed with $V_{max} = 0.2$ $\mu$M s$^{-1}$, $K_m = 0.15$ $\mu$M, i.e., standard Michaelis-Menten parameters, and corresponds to the upper graph of Fig. 7, but with different time and distance scales. The middle graph was computed with $V_{max} = 0.2$ $\mu$M s$^{-1}$, $K_m = 6.0$ $\mu$M, i.e., standard nomifensine parameters. The bottom graph was computed with $V_{max} = 0$, i.e., with no uptake. See legend to Fig. 2 for standard parameters.

because measurement levels will always be significantly greater than $K_m$ unless an uptake blocker is used. Because of this, fourfold differences in $K_m$ have almost no impact when concentrations are in the tens of $\mu$M, as is the case for $I = 100$ nA (Fig. 9 *A*). When concentrations are of the order of a $\mu$M ($I = 20$ nA), fourfold differences in $K_m$ might be detected under ideal conditions (Fig. 9 *B*). When an uptake blocker is applied and $K_m$ increases to a value of several $\mu$M, then it should be possible to determine both $V_{max}$ and $K_m$.

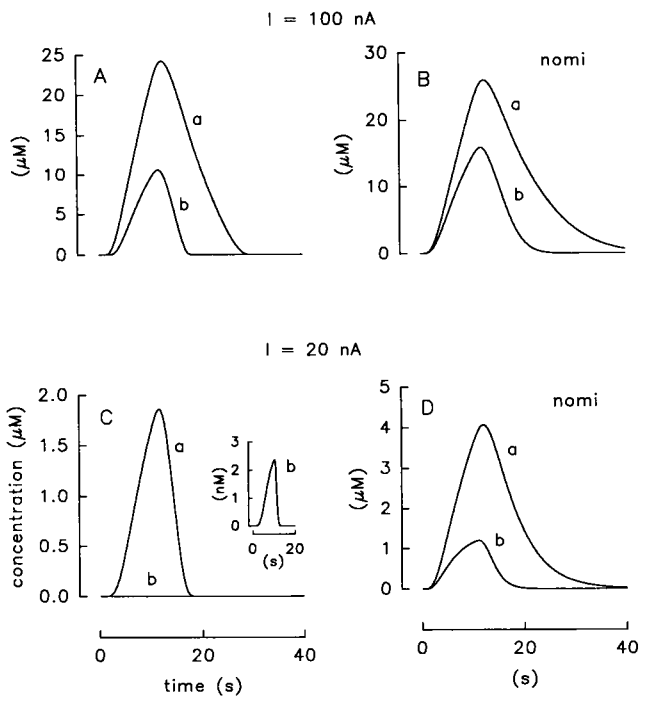


FIGURE 8 Effect of source current on concentration versus time curves for different uptake kinetics. These figures show the nonlinear scaling of curves with source current. All calculations are based on a numerical solution of Eq. 23 with $r$ = 100 μm and an iontophoresis duration of 10 s. For each graph two curves are depicted: curve $a$ used $V_{max}$ = 0.2 μM $s^{-1}$, curve $b$ used $V_{max}$ = 0.8 μM $s^{-1}$. Graph $A$ was computed with $I$ = 100 nA, $K_m$ = 0.15 μM. Graph $B$ was computed with $I$ = 100 nA, $K_m$ = 6.0 μM, i.e., standard nomifensine parameters. Graph $C$ repeats graph $A$ but with one-fifth the source current, i.e., $I$ = 20 nA. The curve with $V_{max}$ = 0.8 μM $s^{-1}$ is now so small that it cannot be seen above the baseline on the concentration scale used, but can be seen on the inset, which uses an expanded scale. Note the change in shape, as well as amplitudes, of the curves here compared with graph $A$. Graph $D$ repeats graph $B$ but with one-fifth the source current, i.e., $I$ = 20 nA. Again note the change in shape, as well as amplitudes, of the curves here compared with graph $B$. See legend to Fig. 2 for standard parameters.

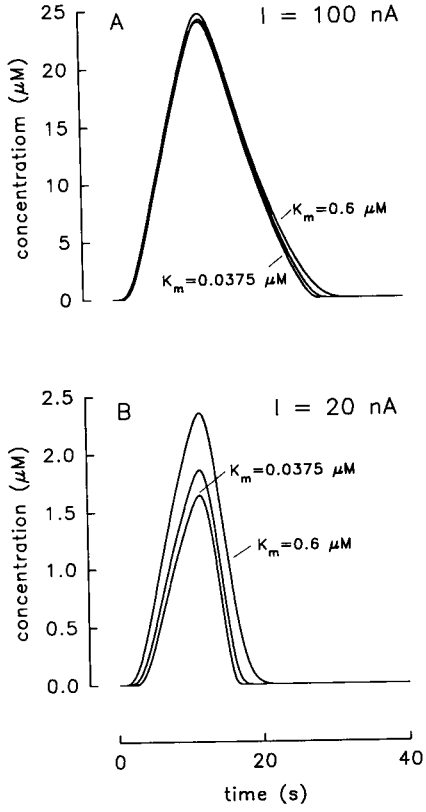


FIGURE 9 Relation between source current, $K_m$, and concentration versus time curves. As source current changes at a given distance, the sensitivity of the concentration to $K_m$ values changes. All calculations are based on a numerical solution of Eq. 23 with $r$ = 100 μm, $V_{max}$ = 0.2 μM $s^{-1}$, and an iontophoresis duration of 10 s. Graph $A$ shows curves for a source current $I$ = 100 nA and $K_m$ values of 0.15 μM (normal value, center curve, not labeled), 0.6 μM (4× normal) and 0.0375 μM (0.25× normal). At these concentration levels, the curves are insensitive to $K_m$. Graph $B$ shows curves for a source current $I$ = 20 nA and the same three $K_m$ values used in Graph $A$. At these concentration levels, the curves demonstrate significant sensitivity to $K_m$. See legend to Fig. 2 for standard parameters.

An experimental strategy suggested by these data is to vary the source strength over a 2- to 10-fold range and attempt to fit the family of curves with a single parameter set. Fig. 10 shows how the amplitude will vary as the current is stepped from 20 to 100 nA and the measurements made 100 μm from the source. The three graphs show the shapes of the curves for three values of $V_{max}$ (0.8, 0.5, and 0.2 μM $s^{-1}$). These plots demonstrate that the amplitudes of the curves are very sensitive to $V_{max}$ (note the different concentration scales), but the shape of the rising edge and time-to-peak of the concentration curves are virtually unaffected by the current increments. The falling phase is sensitive to current, however, and, together with amplitude, this parameter would be useful in determining the curve-fit parameters for the family.

## DISCUSSION

This paper has given a detailed theoretical analysis to show that a method that couples controlled micro-iontophoresis with FCV is able potentially to analyze Michaelis-Menten kinetics in living, intact, brain tissue.

### Classical analysis of Michaelis-Menten kinetics

Many early studies of DA uptake in brain tissue relied on tissue homogenates and fractionation combined with radiolabeled DA, and such methods subsequently have been used extensively to study both kinetics and transport inhibition. For example, Snyder and Coyle (1969) used homogenates, and Holz and Coyle (1974) fractionated the homogenate to obtain synaptosomes. The advantage of these procedures was that the final preparations allowed rapid access of the radiolabeled DA to a suspension of cellular elements, so that the bathing concentration could be defined accurately for the determination of $K_m$, whereas $V_{max}$ could be measured sufficiently rapidly so that the assumption of unidirectional transport was valid. A disadvantage of the homogenate methods was the obliteration of the neuronal circuitry and the microenvironment.

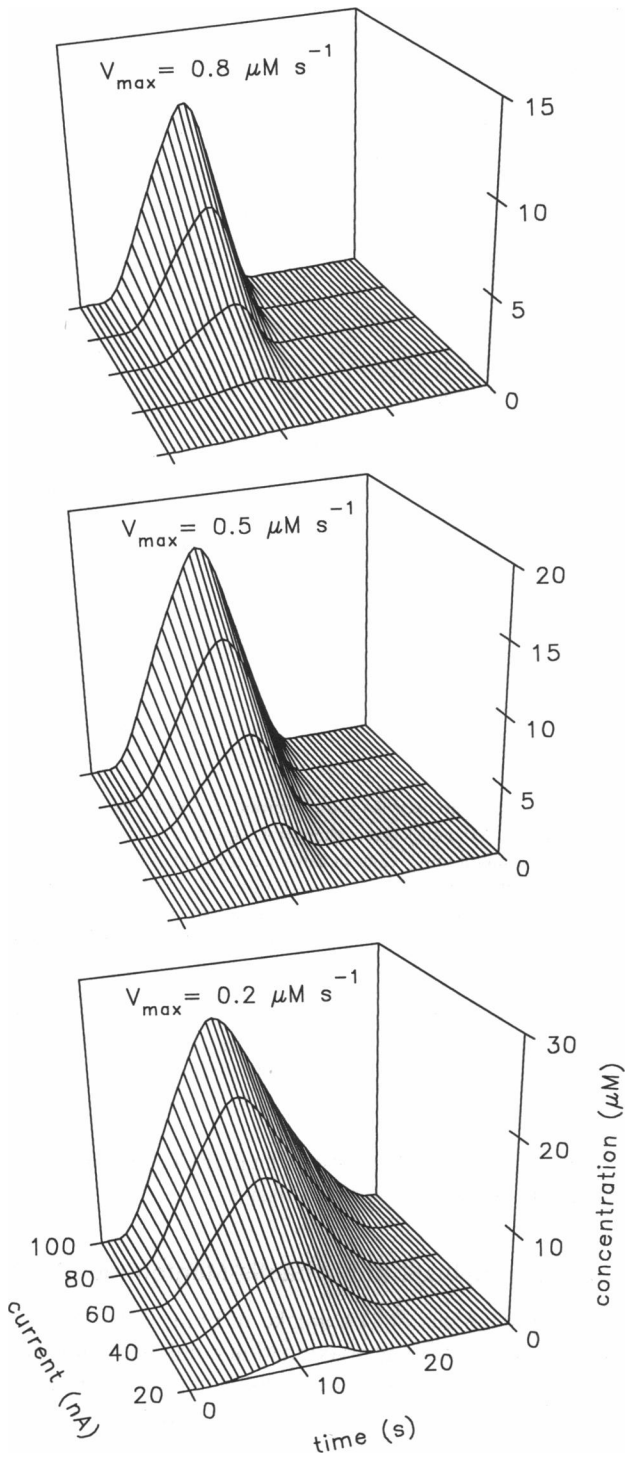


FIGURE 10 Relation between source current and concentration versus time curves for three values of $V_{max}$. As source current changes, the concentration changes at a given distance in a nonlinear manner. All calculations are based on a numerical solution of Eq. 23 and used $r = 100$ μm, $K_m = 0.15$ μM, and an iontophoresis duration of 10 s. In each graph, five source currents were used: $I = 100$, 80, 60, 40, and 20 nA. In the upper graph, $V_{max} = 0.8$ μM $s^{-1}$; in the center graph, $V_{max} = 0.5$ μM $s^{-1}$; and in the lower graph, $V_{max} = 0.2$ μM $s^{-1}$. Note the differences in concentration scales for the three graphs and the differences in shape of the falling surfaces of the graphs. See legend to Fig. 2 for standard parameters.

The use of brain slices exposed to radiolabeled DA overcame the problem of tissue disruption but prevented precise knowledge of extracellular concentrations of substrate throughout the tissue and also severely compromised the ability to deliver substrate quickly to the surface of cellular elements in much of the preparation. The reasons for these uncertainties are obvious from the analysis of this paper; the combination of diffusion and uptake retards the penetration of labeled DA into the slice in a complex, concentration-dependent, manner. Near et al. (1988) have shown that failure to appreciate this issue can lead to the apparent discovery of low affinity (high $K_m$) uptake systems when slices are used, which are not seen in the homogenized preparations. Such low affinity uptake systems were reported by Shaskan and Snyder (1970) and Mireylees et al. (1986) using slices, and the problems of analyzing Michaelis-Menten kinetics in the presence of diffusion were discussed in a theoretical paper by Green (1976).

The use of FCV in intact tissue has the potential to remove the limitations imposed by the traditional methods. Early studies (Stamford et al., 1984, 1986) with FCV actually were interpreted as indicating the presence of both a low and a high affinity uptake systems in the striatum, but this was not found in later and more precise work (see Wightman and Zimmerman (1990) for review). Two limitations of the FCV studies have been difficulty in defining the geometry of the source and lack of sensitivity to physiological DA concentrations. The source of DA has been a population of electrically stimulated fibers (usually the median forebrain bundle) that released DA from their terminals. This has the merit of providing a reasonably physiological source of DA, but the disadvantage that the spatial distribution and behavior of the population of stimulated endings cannot be defined precisely. The lack of sensitivity of FCV arises because the method sacrifices sensitivity for speed so that, even with various recent improvements (Rice and Nicholson, 1989; Wiedemann et al., 1991), it is not possible to detect concentrations of DA in the brain below about 100 nM; in practice, most FCV studies have been carried out with DA concentrations around 1 μM. This makes it difficult to accurately determine $K_m$, which typically has a value of about 150 nM. In the presence of an uptake blocker, such as nomifensine, $K_m$ increases sufficiently to be measured with FCV.

The method described here overcomes problems with the definition of the source, but the issue of sensitivity remains. Thus, presently the combination of iontophoresis and FCV is best suited to the measurement of $V_{max}$. Interestingly, where $V_{max}$ has been estimated by FCV in the anesthetized whole animal preparation (Wightman and Zimmerman, 1990), the parameter often has been found larger than in homogenates.

## Diffusion and Michaelis-Menten kinetics

For an iontophoresis paradigm, this paper has shown how diffusion in a complex medium, characterized by a volume fraction and tortuosity, can be coupled to a Michaelis-

Menten uptake process. This is probably the simplest and most widely accepted nonlinear description of uptake kinetics and has the merit that it only requires two parameters, $V_{max}$ and $K_m$, but it may be an oversimplification. More elaborate models have attempted to take account of the accumulation of DA inside cells and consequent outward transport (Christensen, 1975), but such models are not commonly used because of the additional parameters required. In fact, once a numerical approach is adopted, it is relatively easy to incorporate more complex kinetics, if experimental data justify their use.

The algorithm derived for the solution of the nonlinear partial differential equation is based on the work of Tosaka and Miyake (1982) in the context of oxygen transport in tissue. As noted above, some earlier numerical solutions to the oxygen problem were in error. For this reason, an effort has been made in this paper to compare numerical results with limiting analytical solutions. These solutions also provided insight into the nature of the problem. For example, the case of $C \gg K_m$ ($U \gg K$) leads to a so-called free boundary problem in the steady-state, which has been the subject of extensive analysis in other contexts (Crank, 1984).

The integral-equation approach to the numerical algorithm has the merit of providing a basis for further analytical insights into the mechanics of the problem but at the cost of requiring some analytical derivation for each case. For example, to extend the analysis to a pressure-ejection source instead of an iontophoretic source, it would be necessary to deal with the singularity at the origin. An alternative method of solving this type of problem is the collocation method (Eilbeck, 1983; Lin, 1979; Schultz and King, 1987), which offers a more mechanical approach but less illumination of the solution process and at some risk of generating nonphysiological results.

## Relations between steady-state solutions and time-dependent case

It is instructive to compare some of the simplest solutions that arise from the problem studied here. For a pure diffusion problem with a point source of strength $Q$, the steady-state solution is (e.g., limit of Eq. 45 as $\kappa \to \infty$):

$$C = \frac{Q}{4\pi\alpha D^* r}. \tag{48}$$

If linear concentration-dependent uptake, defined by $k'$, is present, this solution is modified to be (Eq. 45):

$$C = \frac{Q}{4\pi\alpha D^* r} \exp\left(-r\sqrt{\frac{k'}{D^*}}\right). \tag{49}$$

In both cases, the steady-state distribution extends to infinity, although obviously in practice boundaries and the detection limits of instruments or receptor sites impose finite limits. For the nonlinear uptake considered here, as $K_m \to 0$ the situation is different: beyond a certain distance, no diffusing molecules are encountered. One might say that the often-used phrase "diffusion distance" only has meaning in the presence of nonlinear uptake. This is exemplified by the case of the free-boundary solution ($K_m = 0$), where the concentration is zero (Eq. 29, neglecting $r_o^3$) for all $r$ satisfying

$$r \geq \left[\frac{3Q}{4\pi V_{max}}\right]^{1/3}. \tag{50}$$

When $K_m > 0$, however, diffusing particles extend beyond this boundary, although for practical purposes of detection, the concentration may be essentially zero.

As shown in Fig. 4, this situation is reached quite rapidly for DA, with the parameters used here, within a minute or so of the source becoming active. Of course, in the more realistic example shown in Fig. 4, the boundary extends beyond the limit given by Eq. 50 because $K_m > 0$. When the full time-dependent case is considered, DA moves out to a space-time locus where it can no longer be detected and then recedes, much like a tide running up an inclined beach. This is most obvious in Figs. 6 and 7.

## Analysis of data using iontophoresis and FCV

The results depicted in Figs. 8–10 represent data that might be gathered in a typical experiment. The major point made by these simulations is that analysis of nonlinear diffusion-uptake processes is best done using a family of curves. An iontophoretic source is able to generate such a family by varying the current strength, and this gives it advantages over other methods where the source is less easily controlled. As Fig. 10 demonstrates, the issue then becomes one of generating a series of concentration surfaces as functions of time and current, and determining which value of $V_{max}$ generates the surface that fits most closely the experimental data. When measuring techniques of sufficient sensitivity become available, this method could also be applied to determine $K_m$.

Finally, it evident that, so long as appropriate sensors could be found, the approach described here could be applied to many other neuroactive substances to quantify their behavior in situ and in localized regions.

I thank Dr. Lian Tao and Mr. Kuang-Wen Tsao for implementing the numerical tests of the work of Tosaka and Miyake and Dr. Margaret Rice for many valuable comments.

This work was supported by National Institutes of Health grant NS 28642.

## REFERENCES

Anderson, N., and A. M. Arthurs. 1980. Complementary variational principles for diffusion problems with Michaelis-Menten kinetics. *Bull. Math. Biol.* 42:131–135.

Aris, R. 1975. The Mathematical Theory of Diffusion and Reaction in Permeable Catalysts. Vol. 1. The Theory of the Steady State. Clarendon Press, Oxford. 444 pp.

Bach-y-Rita, P. 1993. Nonsynaptic diffusion neurotransmission (NDN) in the brain. *Neurochem. Int.* 23:297–318.

Berg, H. C. 1993. Random Walks in Biology. Expanded Edition. Princeton University Press, Princeton, NJ. 152 pp.

Carslaw, H. S., and J. C. Jaeger. 1959. Conduction of Heat in Solids, 2nd Ed. Clarendon Press, New York. 510 pp.

Cass, W. A., N. R. Zahniser, K. A. Flach, and G. A. Gerhardt. 1993. Clearance of exogenous dopamine in rat dorsal striatum and nucleus accumbens: role of metabolism and effects of locally applied uptake inhibitors. *J. Neurochem.* 61:2269–2278.

Chaplain, M. A. J., and A. M. Stuart. 1991. A mathematical model for the diffusion of tumour angiogenesis factor into the surrounding host tissue. *IMA J. Math. Appl. Med. Biol.* 8:191–220.

Christensen, H. N. 1975. Biological Transport, 2nd Ed. W. A. Benjamin, Reading, MA. 107–165.

Crank, J. 1984. Free and Moving Boundary Problems. Clarendon Press, Oxford. 425 pp.

Cserr, H. F., M. DePasquale, C. Nicholson, C. S. Patlak, K. D. Pettigrew, and M. E. Rice. 1991. Extracellular volume decreases while cell volume is maintained by ion uptake in rat brain during acute hypernatremia. *J. Physiol.* 442:277–295.

Eilbeck, J. C. 1983. A collocation approach to the numerical calculation of simple gradients in reaction-diffusion systems. *J. Math. Biol.* 16: 233–249.

Fuxe, K., and L. F. Agnati, editors. 1991. Volume Transmission in the Brain. Advances in Neuroscience, Vol. 1. Raven Press, New York. 602 pp.

Garris, P. A., and R. M. Wightman. 1994a. Different kinetics govern dopaminergic transmission in the amygdala, prefrontal cortex, and striatum: an in vivo voltammetric study. *J. Neurosci.* 14:442–450.

Garris, P. A., and R. M. Wightman. 1994b. Uptake is the primary mechanism for the extracellular clearance of evoked dopamine in the basolateral amygdaloid nucleus. *Soc. Neurosci. Abstr.* 20:282.

Garris, P. A., E. L. Ciolkowski, and R. M. Wightman. 1994. Heterogeneity of evoked dopamine overflow within the striatal and striatoamygdaloid regions. *Neuroscience.* 59:417–427.

Gerhardt, G., and R. N. Adams. 1982. Determination of diffusion coefficients by flow injection analysis. *Anal. Chem.* 54:2618–2620.

Gray, W. G., and P. C. Y. Lee. 1977. On the theorems for local volume averaging of multiphase systems. *Int. J. Multiphase Flow.* 3:333–340.

Green, A. L. 1976. The kinetics of enzyme action and inhibition in intact tissues and tissue slices, with special reference to cholinesterase. *J. Pharm. Pharmacol.* 28:265–274.

Hille, B. 1992. G protein-coupled mechanisms and nervous signaling. *Neuron.* 9:187–195.

Hiltmann, P., and P. Lory. 1983. On oxygen diffusion in a spherical cell with Michaelis-Menten oxygen uptake kinetics. *Bull. Math. Biol.* 45:661–664.

Hitri, A., Y. L. Hurd, R. J. Wyatt, and S. I. Deutsch. 1994. Molecular, functional and biochemical characteristics of the dopamine transporter: regional differences and clinical relevance. *Clin. Neuropharmacol.* 17: 1–22.

Holz, R. W., and J. T. Coyle. 1974. The effects of various salts, temperature, and the alkaloids veratridine and batrachotoxin on the uptake of [$^3$H]-dopamine into synaptosomes from rat striatum. *Mol. Pharmacol.* 10: 746–758.

Horn, A. S. 1979. Characteristics of dopamine uptake. *In* The Neurobiology of Dopamine. A. S. Horn, J. Korf, and B. H. C. Westerink, editors. Academic Press, London. 217–235.

Horn, A. S. 1990. Dopamine uptake: a review of progress in the last decade. *Prog. Neurobiol.* 34:387–400.

Isaacson, J. S., J. M. Solis, and R. A. Nicoll. 1993. Local and diffuse synaptic actions of GABA in the hippocampus. *Neuron.* 10:165–175.

Justice, J. B., L. C. Nicolaysen, and A. C. Michael. 1988. Modeling the dopaminergic nerve terminal. *J. Neurosci. Methods.* 22:239–252.

Katzman, R., and H. M. Pappius. 1973. Brain Electrolytes and Fluid Metabolism. Williams & Wilkins, Baltimore, MD. 419 pp.

Kawagoe, K. T., P. A. Garris, D. J. Wiedemann, and R. M. Wightman. 1992. Regulation of transient dopamine concentration gradients in the microenvironment surrounding nerve terminals in the rat striatum. *Neuroscience.* 51:55–64.

Kelly, R. S., and R. M. Wightman 1987. Detection of dopamine overflow and diffusion with voltammetry in slices of rat brain. *Brain Res.* 423: 79–87.

Kennedy, R. T., S. R. Jones, and R. M. Wightman. 1992a. Dynamic observation of dopamine autoreceptor effects in rat striatal slices. *J. Neurochem.* 59:449–455.

Kennedy, R. T., S. R. Jones, and R. M. Wightman. 1992b. Simultaneous measurement of oxygen and dopamine: coupling of oxygen consumption and neurotransmission. *Neuroscience.* 47:603–612.

Lin, S. H. 1976. Oxygen diffusion in a spherical cell with nonlinear oxygen uptake kinetics. *J. Theor. Biol.* 60:449–457.

Lin, S. H. 1979. Nonlinear diffusion in biological systems. *Bull. Math. Biol.* 41:151–162.

Luthman, J., M. N. Friedemann, B. J. Hoffer, and G. A. Gerhardt. 1993. In vivo electrochemical measurements of exogenous dopamine clearance in normal and neonatal 6-hydroxydopamine-treated rat striatum. *Exp. Neurol.* 122:273–282.

May, L. J., W. G. Kuhr, and R. M. Wightman. 1988. Differentiation of dopamine overflow and uptake processes in the extracellular fluid of the rat caudate nucleus with fast-scan in vivo voltammetry. *J. Neurochem.* 51:1060–1069.

McElwain, D. L. S. 1978. A re-examination of oxygen diffusion in a spherical cell with Michaelis-Menten oxygen uptake kinetics. *J. Theor. Biol.* 71:255–263.

Mireylees, S. E., N. T. Brammer, and G. A. Buckley. 1986. A kinetic study of the in vitro uptake of [$^3$H]dopamine over a wide range of concentrations by rat striatal preparations. *Biochem. Pharmacol.* 35:4065–4071.

Near, J. A., J. C. Bigelow, and R. M. Wightman. 1988. Comparison of uptake of dopamine in rat striatal chopped tissue and synaptosomes. *J. Pharmacol. Exp. Ther.* 245:921–927.

Nicholson, C. 1979. Brain cell microenvironment as a communication channel. *In* The Neurosciences Fourth Study Program. F. O. Schmitt and F. G. Worden, editors. MIT Press, Cambridge, MA. 457–476.

Nicholson, C. 1985. Diffusion from an injected volume of substance in brain tissue with arbitrary volume fraction and tortuosity. *Brain Res.* 333: 325–329.

Nicholson, C. 1992. Quantitative analysis of extracellular space using the method of $TMA^+$ iontophoresis and the issue of $TMA^+$ uptake. *Can. J. Physiol. Pharmacol.* 70:S314–S322.

Nicholson, C., and J. M. Phillips 1981. Ion diffusion modified by tortuosity and volume fraction in the extracellular microenvironment of the rat cerebellum. *J. Physiol.* 321:225–257.

Nicholson, C., and M. E. Rice 1991. Diffusion of ions and transmitters in the brain cell microenvironment. *In* Volume Transmission in the Brain: Novel Mechanisms for Neural Transmission. Advances in Neuroscience, Vol. 1. K. Fuxe and L. F. Agnati, editors. Raven Press, New York. 279–294.

Press, W. H., B. P. Flannery, S. A. Teukolsky, and W. T. Vetterling. 1986. Numerical Recipes. University Press, Cambridge. 818 pp.

Rice, M. E., and C. Nicholson. 1989. Measurement of nanomolar dopamine diffusion using low-noise perfluorinated ionomer coated carbon fiber microelectrodes and high-speed cyclic voltammetry. *Anal. Chem.* 61: 1805–1810.

Rice, M. E., and C. Nicholson. 1991. Diffusion characteristics and extracellular volume fraction during normoxia and hypoxia in slices of rat neostriatum. *J. Neurophysiol.* 65:264–272.

Rice, M. E., and C. Nicholson. 1995. Diffusion and ion shifts in the brain extracellular microenvironment and their relevance for voltammetric measurements. *In* Neuromethods, Vol. 27 Voltammetric Methods. A. A. Boulton, G. B. Baker, and R. N. Adams, editors. Humana Press, Totowa, NJ. 27–79.

Ross, S. B. 1991. Synaptic concentration of dopamine in the mouse striatum in relationship to the kinetic properties of the dopamine receptors and uptake mechanism. *J. Neurochem.* 56:22–29.

Roughton, F. J. W. 1932. Diffusion and chemical reaction velocity as joint factors in determining the rate of uptake of oxygen and carbon monoxide by the red blood corpuscle. *Proc. R. Soc. Lond. Series B.* 111:1–36.

Roughton, F. J. W. 1952. Diffusion and chemical reaction velocity in cylindrical and spherical systems of physiological interest. *Proc. R. Soc. Lond. Series B.* 203–229.

Rubinow, S. I. 1975. Introduction to Mathematical Biology. John Wiley & Sons, New York. 386 pp.

Schmitt, F. O. 1984. Molecular regulators of brain functioning: a new view. *Neuroscience.* 13:991–1001.

Schoemaker, H., and V. J. Nickolson. 1983. Dopamine uptake by rat striatal synaptosomes: a compartmental analysis. *J. Neurochem.* 41:684–590.

Schultz, D. S., and W. E. King. 1987. On the analysis of oxygen diffusion and reaction in biological systems. *Math. Biosci.* 83:179–190.

Schuman, E. M., and D. V. Madison 1994. Locally distributed synaptic potentiation in the hippocampus. *Science.* 263:532–536.

Shaskan, E. G., and S. H. Snyder. 1970. Kinetics of serotonin accumulation into slices from rat brain: relationship to catecholamine uptake. *J. Pharmacol. Exp. Ther.* 175:404–418.

Snyder, S. H., and J. T. Coyle. 1969. Regional differences in [$H^3$]norepinephrine and [$H^3$]dopamine uptake into rat brain homogenates. *J. Pharmacol. Exp. Ther.* 165:78–86.

Stamford, J. A., Z. L. Kruk, and J. Millar. 1986. In vivo voltammetric characterization of low affinity striatal dopamine uptake. I. Inhibition profile and relation to dopaminergic innervation density. *Brain Res.* 373: 85–91.

Stamford, J. A., Z. L. Kruk, J. Millar, and R. M. Wightman. 1984. Striatal dopamine uptake in the rat: in vivo analysis by fast cyclic voltammetry. *Neurosci. Lett.* 51:133–138.

Tosaka, N., and S. Miyake. 1982. Analysis of nonlinear diffusion problem with Michaelis-Menten kinetics by an integral equation method. *Bull. Math. Biol.* 44:841–849.

Van Horne, C., B. J. Hoffer, I. Strömberg, and G. A. Gerhardt. 1992. Clearance and diffusion of locally applied dopamine in normal and 6-hydroxydopamine-lesioned rat striatum. *J. Pharmacol. Exp. Ther.* 263: 1285–1292.

Wiedemann, D. J., K. T. Kawagoe, R. T. Kennedy, E. L. Ciolkowski, and R. M. Wightman. 1991. Strategies for low detection limit measurements with cyclic voltammetry. *Anal. Chem.* 63:2965–2970.

Wightman, R. M., and J. B. Zimmerman. 1990. Control of dopamine extracellular concentration in rat striatum by impulse flow and uptake. *Brain Res. Rev.* 15:135–144.

Wightman, R. M., C. Amatore, R. C. Engstrom, P. D. Hale, E. W. Kristensen, W. G. Kuhr, and L. J. May. 1988. Real-time characterization of dopamine overflow and uptake in the rat striatum. *Neuroscience.* 25:513–523.

Winn, S. R., L. Wahlberg, P. Tresco, and P. Aebischer. 1989. An encapsulated dopamine-releasing polymer alleviates experimental parkinsonism in rats. *Exp. Neurol.* 105:244–250.

Zigmond, M. J., T. G. Hastings, and E. D. Abercrombie. 1992. Neurochemical responses to 6-hydroxydopamine and L-dopa therapy: implications for Parkinson's disease. *Ann. NY Acad. Sci.* 648:71–86.

Zimányi, I., A. Lajtha, and M. E. A. Reith. 1989. Comparison of characteristics of dopamine uptake and mazindol binding in mouse striatum. *Naunyn-Schmiedebergs Arch. Pharmacol.* 340:626–632.